Journal of Mechatronics Engineering

Antipodal Vivaldi Antenna with Star Trek insignia-based side slot edge for ultra-wideband applications

RAIMUNDO EIDER FIGUEREDO[1], ALEXANDRE MANIÇOBA DE OLIVEIRA[1,2], JOÃO FRANCISCO JUSTO 3[1,3]

[1]Microwave Maxwell Laboratory and Applied Electromagnetism (LABMAX)
[2]Federal Institute of São Paulo (IFSP)
[3]Department of Electronic Systems Engineering at the Polytechnic School of the University of São Paulo

<raimundo@labmax.org>, <amanicoba@labmax.org>, <jjusto@lme.usp.br>

DOI: 10.21439/jme.v6i1.112

Received: July 6th, 2023. **Accepted:** November 5th, 2023

Abstract. This article presents a Vivaldi Antipodal Antenna (AVA) with lens and radiating side cavities based on the Star Trek insignia, called Star Trek Side Edge Radiation (STSER-AVA). The objective was to improve parameters to make the radiation of the proposed antenna more directive. To this aim, the development is focused on reducing the squint of the central radiation beam and the side lobe level (SLL), as well as increasing the gain compared to a Conventional AVA. To achieve the objective, using an optimized design. The proposed antenna with or without a lens reached the target with a squint of -2.0 degrees, at 3.90 GHz the antenna with a lens achieved better gain (9.42 dB), but with a greater reduction in SLL of -10.73 dB compared to the lens less antenna. The results were obtained with computational electromagnetic simulations and experimental measurements.

Keywords: Microwave, Planar antennas, Side lobe level.

1 Introduction

Antennas are devices that could present ultrawide bandwidth (UWB) characteristics, enabling various applications, such as wireless communication (DIXIT; KUMAR, 2020a; TENI et al., 2013; CHOUKIKER; SHARMA; BEHERA, 2013), signal jammers (blockers signs) (TENI et al., 2013), satellite communication (NASSAR; WELLER, 2015), radars (BOURQUI; OKONIEWSKI; FEAR, 2010; OLIVEIRA et al., 2019), medical microwave tomography (BOURQUI; OKONIEWSKI; FEAR, 2010; OLIVEIRA et al., 2019; SOBRINHO et al., 2020; FIGUEREDO et al., 2020b) and 5G communication (FEI et al., 2011).

The Antipodal Vivaldi Antenna (AVA), which is the basis of this study, has vast applicability in UWB systems, as several techniques have been devised to breed the radiation parameters of conventional AVA. The techniques are: array of AVA (DIXIT; KUMAR, 2020a), Balanced AVA with and without a director (OLIVEIRA et al., 2019), dielectric lenses and zero index material (NASSAR; WELLER, 2015; BOURQUI; OKONIEWSKI; FEAR, 2010), rectangular and triangular resonant cavities (TENI et al., 2013; FEI et al., 2011) and radiators with exponential and fractal curves (OLIVEIRA et al., 2019; SOBRINHO et al., 2020; FIGUEREDO et al., 2020b).

The technique that uses resonant side cavities (slots) highlights the RSE (Regular Slot Edge), which are rectangular cavities, and the TSE (Tapered Slot Edge), which are triangular. This method causes a reduction in SLL (BAI; SHI; PRATHER, 2011), operating frequency, improved directivity (FEI et al., 2011), and antenna co-polarization (DIXIT; KUMAR, 2020b). The resonant slots increase the electrical length and reduce the physical size, being able to generate inductance and

capacitance in the antennas (DIXIT; KUMAR, 2020a). To achieve this, the RSE works as an equivalent RLC resonator circuit (FEI et al., 2011) and, like the TSE, it confines the electric fields in its cavities, causing a decrease in efficiency (OLIVEIRA et al., 2015; FEI et al., 2011).

There is also another technique in which the cavities are radiant and which is called ESE (Exponential Slot Edge) (OLIVEIRA et al., 2015), which uses cavities with exponential curves, and FSE (Fractal Slot Edge) (FIGUEREDO et al., 2020b; OLIVEIRA et al., 2017; BAI; SHI; PRATHER, 2011; FIGUEREDO et al., 2022; FIGUEREDO et al., 2020; FIGUEREDO et al., 2020a; FIGUEREDO et al., 2021), which uses fractal geometries in which the cavities act as parasitic antennas (OLIVEIRA et al., 2017), controlling the currents at the edges of the AVA and channeling them to the main radiator, the which results in a decrease in SLL and an increase in gain simultaneously (OLIVEIRA et al., 2015).

Because this work proposes the use of a lens, it is important to mention the AVA with the director (NASSAR; WELLER, 2015), which is located in the centre of the main exponential radiator of the AVA, functioning as a waveguide that directs the energy to the centre in a similar way to the lens, as a consequence, the director reduces the phase speed of the electromagnetic waves about the main radiator (BOURQUI; OKONIEWSKI; FEAR, 2010), improves the gain (ZHU et al., 2018), bandwidth and directivity about conventional AVA (NASSAR; WELLER, 2015).

There is a technique as previously mentioned that makes use of dielectric lenses and metamaterials (NASSAR; WELLER, 2015), (ZHU et al., 2018) resulting in an improvement in directivity, gain, and a decrease in SLL (TENI et al., 2013; OLIVEIRA et al., 2019; ZHU et al., 2018; DIXIT; KUMAR, 2020b) and greater radiation stability across the entire bandwidth (TENI et al., 2013).

This work proposes to use radiant cavities at the side edges of the conventional AVA, as such cavities can control the surface currents of the edges and direct them to the main exponential radiative of AVA (OLIVEIRA et al., 2019; SOBRINHO et al., 2020) unlike resonant cavities that behave like an RLC circuit (FEI et al., 2011). The geometry applied to side edges and the lens was based on the Star Trek logo to reduce strabismus and side lobe level (SLL) and increase the gain.

The work implements two techniques in the AVA, radiant cavities and dielectric lenses, with geometries that were not identified in use in the AVA. The production of a hybrid model, which uses two construction techniques, contributes to uniting the improvement characteristics of these two techniques. The results demonstrated that there is an improvement in terms of squint, gain, and SLL, which is precisely what the work proposes to do.

The article is divided into four sections: Section II, presents the methodology used for the development of the proposed antenna; Section III presents the results found in the computational environment and measurements and, Section IV presents the conclusions.

2 Development of antennas

All development and tests to verify the viability of the proposed antenna were performed using the Ansys HFSS 2021 software, in which the FR-4 substrate model was the Dielectric Constant 3.5 with dimensions 1.6 x 150.0 x 150.0 mm^3 and an SMA impedance of 50 Ω in correspondence to the transmission line of the AVA and the proposed antenna, labeled Star Trek Slot Edge Radiation (STSER-AVA).

The choice of horizontal geometry at a right angle and another with an angle of 20º (Figure 1) were applied to mix the two characteristics in one, to increase the carved area at the edges of the antenna to reduce the currents on the sides, as well as the pointed geometries that are explained by the theory of tips the load accumulation precisely at the ends. AVA and STSER- AVA dimensions parameters are presented in Figure 1 (a) and (b), respectively, while in Figure 1 (c) these are the side cavities of STSER-AVA.

Table 1 presents the dimensions of Figure 1 with the values of parameters a, b, c, d, e. Also, w_1, w_1, and r are the same for AVA and STSER-AVA, while f, g, h, i, j, and k are exclusive to STSER-AVA.

The lens was designed in a CAD environment, where Figure 2 presents the respective dimensions. The lens was made of PLA with a 3.5 dielectric constant (HUBER et al., 2016) using Ender Creality additive manufacturing with erectility filling configurations and 100% density and 1.6 mm thickness to the lens and 1.0 mm to a smaller part than connecting the lens to an antenna.

For STSER-AVA and AVA, prototyping was done in 8 steps using a chemical attack technique. The steps are presented below and are in chronological order:

Step 1: Graphic designer and printing of models;

Step 2: Designer clipping on substrate copper blade;

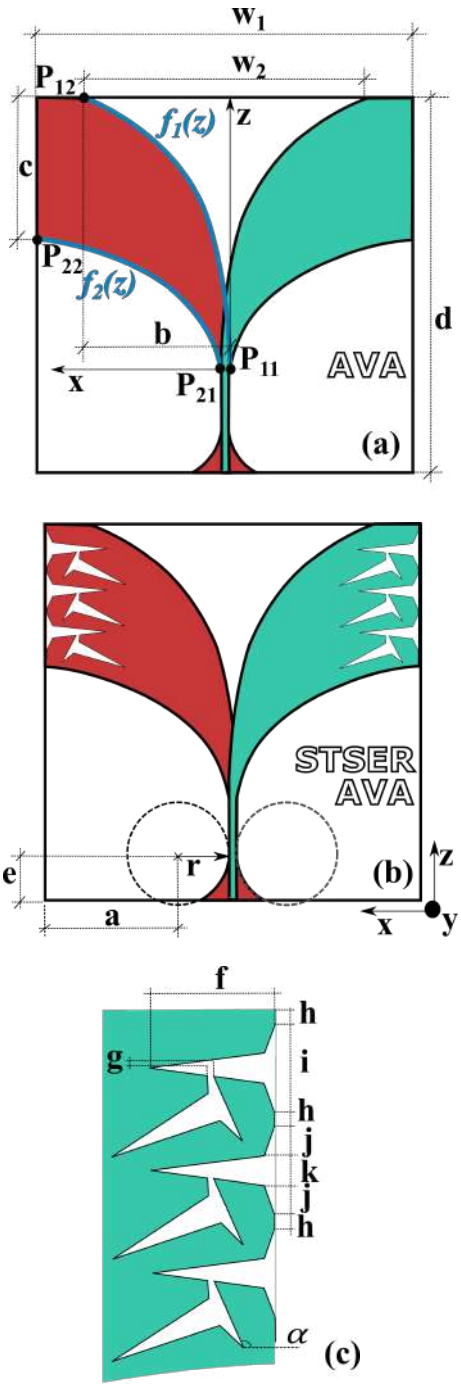

Figure 1: Parameter and dimensions of AVA (a), STSER-AVA (b), (c) caves of STSER-AVA.

Table 1: Parameters and dimensions of AVA and STSER-AVA.

Parameters	Dimensions [mm]
a	53.50
b	58.36
c	55.00
d	150.00
e	18.10
f	22.00
g	1.10
h	2.00
i	15.00
j	5.00
k	5.00
r	20.00
w_1	150.00
w_2	113.71
α 20º	

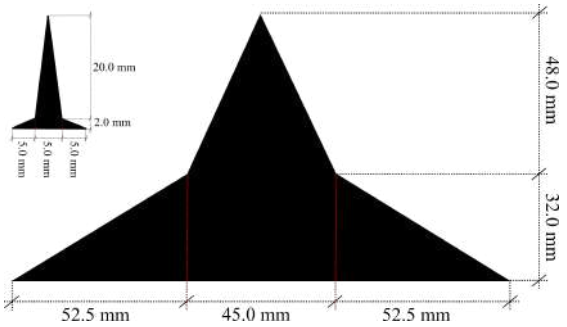

Figure 2: Lens dimensions in PLA.

Step 3: Application of the aqueous perchloride solution to the corrosion plate;

Step 4: Washing plate for removal of excess perchloride;

Step 5: Application of sodium bicarbonate solution to cease corrosion from step 3;

Step 6: Dry the plates that are now the prototyped antennas;

Step 7: Welding with a tin alloy of 50 Ω SMA connectors on the antennas;

Step 8: Application of varnish in the copper layer of the antennas to avoid oxidation of the metal part of the antenna.

The result of STSER-AVA prototyping is presented in the upper part of Figure 3 (a) without a lens, (b) the bottom (GND) with a lens, and (c) the cavities of STSER-AVA.

To measure the S_{11} parameter of the antennas, a NanoVNA V2 was used with frequency analysis between 0.15 and 4.0 GHz with 200 points in environmental conditions of the location with a temperature of 25ºC and relative humidity of 39% of the air being assembled in an open environment, free from obstacles, to minimize the effects of external electromagnetic factors. The antenna fixing support used was made of PLA. The entire setup was mounted on a glass table with wooden legs. Figure 4 shows the material used to assemble the setup for measuring the S_{11} parameters using the NanoVNA and the prototyped antennas.

Figure 3: STSER-AVA prototype. (a) upper plan without a lens, (b) lower plane (GND) with a lens, and (c) cavities.

3 Results and discussion

Figure 5 presents the loss due to the return of radiation from AVA and STSER -AVA without and with a lens, where the ideal is below -10 dB (OLIVEIRA et al., 2019). The proposed cavities helped slightly reduce the lower frequency limit (LFL) from a conventional AVA. The LFL of STSER-AVA without a lens was 1.59 GHz, while with a lens and AVA was 1.61 GHz.

Figure 6 presents the gain as a function of frequency, in which the largest peak for STSER-AVA at 3.90 GHz is 8.92 dB using a lens and 8.40 dB without it, while the AVA peak at 3.10 GHz is 7.83 dB. It is possible to check in the chart be- low that STSER-AVA with and without a lens has higher gains compared to AVA also below 2.25 GHz.

Figure 7 presents the radiation diagram at 3.90 GHz for AVA and STSER-AVA with and without a lens. It is possible to verify the strabismus, SLL level, and gain, as viewed by the radiations on the side edges of the pro-

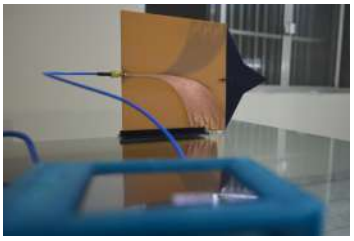

Figure 4: Setup for S_{11} measurement of AVA and STSER-AVA.

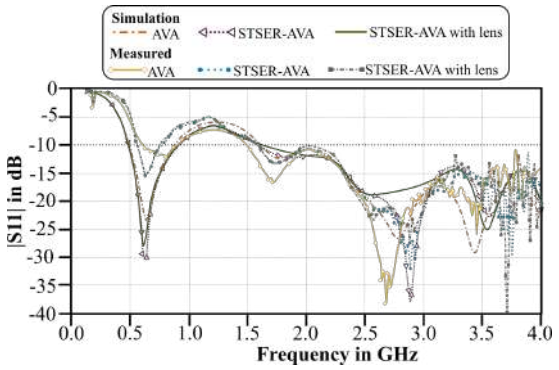

Figure 5: S_{11} of AVA and STSER-AVA with and without a lens.

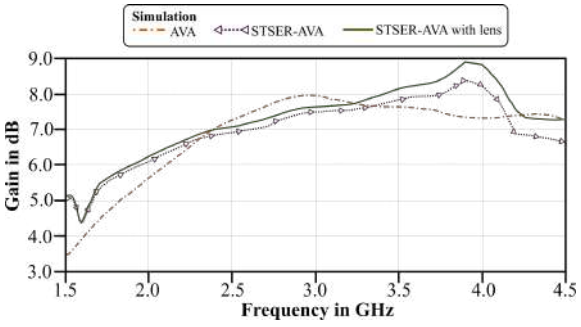

Figure 6: Gain of AVA and STSER-AVA with and without a lens.

posed antennas are lower and directional radiation levels are higher indicating that the proposed system can increase the gain and decrease SLL, while the results are presented in Table 2.

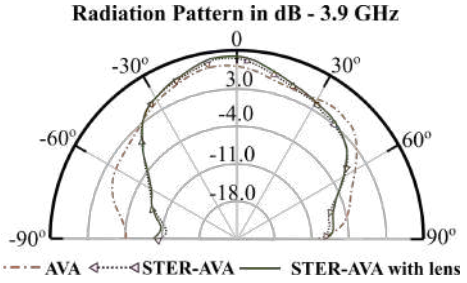

Figure 7: Diagram pattern 2D in 3.90 GHz from AVA and STSER-AVA with and without a lens.

Table 2: Comparison of AVA with STSER-AVA with and without a lens at 3.90 GHz.

Parameters Results	**AVA**	**STSER-AVA**	**STSER-AVA with Lens**
Gain[dB]	7.21	8.40	8.92
SLL[dB]	-4.11	-10.73	-9.42
Strabism [Degree]	-6.00	-2.00	-2.00

The results in Table 2 show that the proposed system presents better results compared to AVA, the cavities are radiant precisely because STSER-AVA increased gain and reduced the SLL levels simultaneously, which defines a Palm Tree class antenna (OLIVEIRA et al., 2019).

Another radiation factor analyzed was the near magnetic field (NHF) and the near electric field (NEF) of the antennas at 3.90 GHz in a 300 mm radius sphere, presented in Figure 8 (a) and (b), respectively. The nearby fields are the short distances where the antennas are resonant it is possible to verify that the proposed antennas levels are slightly higher in the main lobe, indicating a higher resonance than in AVA, but the side levels and the central beam angle of the proposed antennas are smaller.

Figures 9 (a), (b), and (c) show the surface current density in an AVA, and STSER-AVA with and without a lens, respectively, at 3.90 GHz. The currents at STSER-AVA edges are less intense especially when using the lens, which causes SLL reduction and greater current intensity in the exponential radiator, leading to improvement in gain and decrease in central bundle strabis-

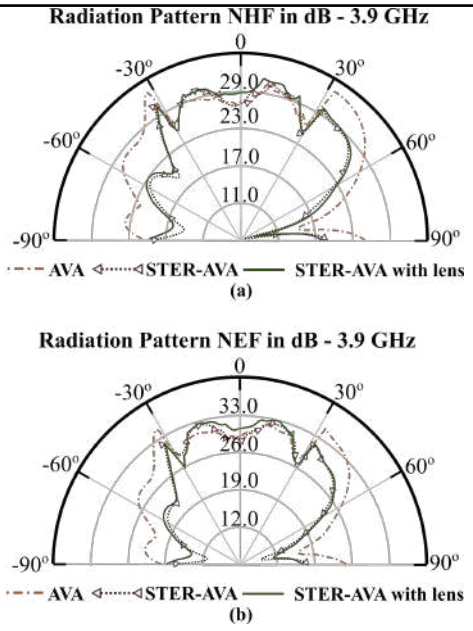

Figure 8: Diagram pattern of near field magnetic (a) and electric (b).

mus radiation. The current on the lens surface is practically null, as shown in Figure 9 (c).

Figure 10 presents the electric field lines acting in AVA, Figure 10 (a), STSER-AVA without, Figure 10 (b), and with a lens, Figure 10 (c). where the pointed tips of geometry at STSER-AVA edges accumulate a large amount of electric field load. In AVA, there is an imbalance between the upper copper surface, on the right side of Figure 10 (a), and the lower one, on the left side of Figure 10 (a), which has low-intensity (blue) space of the fields, this leads to the displacement of the central flex of antenna radiation and strabismus appearing. On the other hand, in the lines of the electric field in the lens presented in Figure 10 (c), there is less density than in the antennas themselves and more spaces, but there is greater density in the ends and transition from a larger area to the smaller lens.

Given the results found in measurements and computer simulations, the ones that attract the most attention are related to the surface currents of the antennas, which have lateral cavities that accumulate a lot of charges at their ends, the radiation diagram that shows a more directive radiation beam and the gain results, strabismus and SLL showing the improvement in the conventional AVA of the proposed antennas.

That said, it is important to emphasize that STSER-

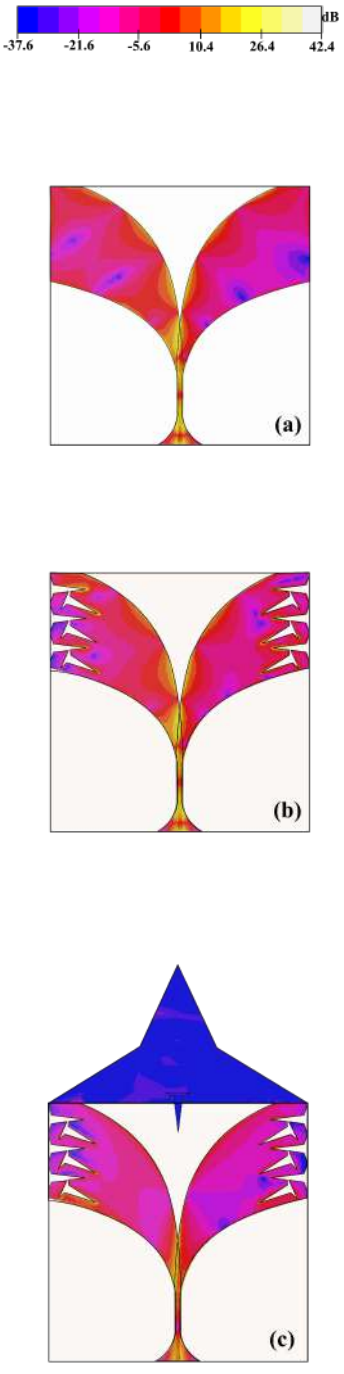

Figure 9: Surface current density at 3.90 GHz of AVA (b) and STSER-AVA (a).

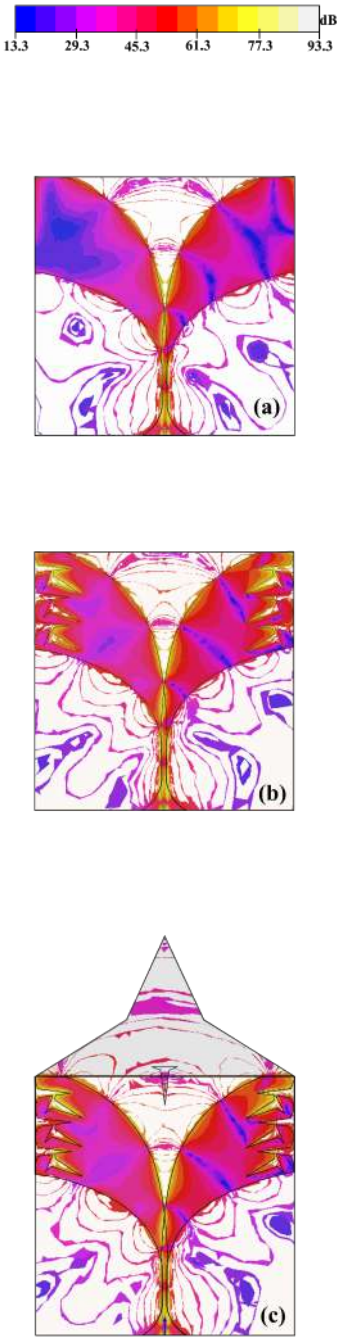

Figure 10: Electric field lines on antennas AVA (a), STSER-AVA without a lens (b) and STSER-AVA with a lens (c) at 3.90 GHz.

AVA with a lens increases the dimensions of the antenna and ends up being uncharacterized, becoming larger than the conventional AVA, where for applications in systems with limited dimensions it will be difficult to use, but the proposed antenna can be used without the lens despite having a lower performance than the lens, but better than the AVA. Another factor is the complexity of using two techniques despite cavities being a simple application technique.

Regarding manufacturing costs, the proposed antenna with a lens costs more than without a lens and the AVA, however, the need for application in a system that requires greater gain and directivity and without space limitations, the antenna with a lens meets the requirements. In cases with limited space and requiring greater gain and directivity and low SLL, STSER-AVA can be used and has costs equal to conversational AVA in its production.

4 Conclusion

The incorporation of side cavities and lens in the AVA has modified the behavior of surface currents and electric fields causing changes in the gain, SLL, S_{11}, and degree of radiation fix. The improvement of these parameters makes the STSER-AVA more directive and less susceptible to electromagnetic interference, which are desirable characteristics in UWB systems.

As it is an antenna operating in UWB and with conventional radiation, as seen in the results obtained, it is possible to consider future work aimed at applying STSER-AVA with and without a lens in radar systems for detecting internal cracks in blades of wind generators that wear out due to air friction and the force of gravity on their structure.

References

BAI, J.; SHI, S.; PRATHER, D. W. Modified compact antipodal vivaldi antenna for 4–50-ghz uwb application. *IEEE Transactions on Microwave Theory and Techniques*, IEEE, v. 59, n. 4, p. 1051–1057, 2011.

BOURQUI, J.; OKONIEWSKI, M.; FEAR, E. C. Balanced antipodal vivaldi antenna with dielectric director for near-field microwave imaging. *IEEE Transactions on Antennas and Propagation*, IEEE, v. 58, n. 7, p. 2318–2326, 2010.

CHOUKIKER, Y. K.; SHARMA, S. K.; BEHERA, S. K. Hybrid fractal shape planar monopole antenna covering multiband wireless communications with

mimo implementation for handheld mobile devices. *IEEE Transactions on Antennas and Propagation*, IEEE, v. 62, n. 3, p. 1483–1488, 2013.

DIXIT, A. S.; KUMAR, S. A miniaturized antipodal vivaldi antenna for 5g communication applications. In: IEEE. *2020 7th international conference on signal processing and integrated networks (SPIN)*. [S.l.], 2020. p. 800–803.

DIXIT, A. S.; KUMAR, S. A survey of performance enhancement techniques of antipodal vivaldi antenna. *Ieee Access*, IEEE, v. 8, p. 45774–45796, 2020.

FEI, P.; JIAO, Y.-C.; HU, W.; ZHANG, F.-S. A miniaturized antipodal vivaldi antenna with improved radiation characteristics. *IEEE antennas and wireless propagation letters*, IEEE, v. 10, p. 127–130, 2011.

FIGUEREDO, R.; OLIVEIRA, A. de; SERRES, A.; ALEXANDRIA, A. R. de; JUSTO, J.; PEROTONI, M. Antipodal vivaldi antenna with radiant side cavities with fractal levy curve. *In: CONFERÊNCIA NACIONAL EM COMUNICAÇÕES, REDES E SEGURANÇA DA INFORMAÇÃO (ENCOM), Natal. Disponível em: <https://iecom.org.br/encom2020/autores.htmlanais*$_s ec >$ *.*, $Anaiseletrnicos.ENCOM$, 2020.

FIGUEREDO, R. E.; OLIVEIRA, A. M. de; NURHAYATI, N.; NETO, A. M. d. O.; NOGUEIRA, I. C.; JUSTO, J. F.; PEROTONI, M. B.; CARVALHO, A. de. A vivaldi antenna palm tree class with koch square fractal slot edge for near-field microwave biomedical imaging applications. In: IEEE. *2020 Third International Conference on Vocational Education and Electrical Engineering (ICVEE)*. [S.l.], 2020. p. 1–6.

FIGUEREDO, R. E.; OLIVEIRA, A. M. de; PINTO, M. A. B.; VICENTINE, G. F.; COSTA, H. G. da; SERRES, A. J.; PEROTONI, M. B.; JUSTO, J. F.; JR, A. de C.; NETO, A. G. Antena vivaldi antipodal com cavidades laterais com geometria fractal de hilbert. *In: WORKSHOP DE MICRO-ONDAS (WMO), Cubatão. Disponível em:< https://labmax.org/index.php/wmo-anais/wmo-anteriores/>.*, 2022.

FIGUEREDO, R. E.; OLIVEIRA, A. M. de; SERRES, A. J. et al. Antipodal vivaldi antenna with side radiating slot edge with sierpinski curve fractals. *in: SIMPOSIO BRASILEIRO DE MICRO-ONDAS E OPTOELETRÔNICA E CONGRESSO BRASILEIRO DE ELETROMAGNETISMO, Rio de Janeiro. Disponível em: < https: //drive.google.com/file/d/ 1awjFbTcpKI-OPFysm7B4sbeM2LxBAcKG/view?ts=602fbb6b >.*, 2020.

FIGUEREDO, R. E.; VICENTINE, G. F.; JR, J. M. D.; MEDEIROS, L. P. G. C. D.; SILVA, G. C. P. D.; PINTO, M. A. B.; ALEXANDRIA, A. R. D.; PEROTONI, M. B.; JUSTOS, J. F.; NURHAYATI, N.; OLIVEIRA, A. M. D. Desenvolvimento de uma antena vivaldi antipodal com cavidades laterais utilizando fractal de sierpinski para melhoramento dos parâmetros de radiação. *In: WORKSHOP DE MICRO-ONDAS (WMO), Disponível em: <https://labmax.org/index.php/wmo-anais/wmo-edicao-atual/>. Acesso em: 04 mai. 2022.*, Anais eletrônicos. WMO, 2021.

HUBER, E.; MIRZAEE, M.; BJORGAARD, J.; HOYACK, M.; NOGHANIAN, S.; CHANG, I. Dielectric property measurement of pla. In: IEEE. *2016 IEEE International Conference on Electro Information Technology (EIT)*. [S.l.], 2016. p. 0788–0792.

NASSAR, I. T.; WELLER, T. M. A novel method for improving antipodal vivaldi antenna performance. *IEEE Transactions on Antennas and Propagation*, IEEE, v. 63, n. 7, p. 3321–3324, 2015.

OLIVEIRA, A. M. D.; PEROTONI, M. B.; KOFUJI, S. T.; JUSTO, J. F. A palm tree antipodal vivaldi antenna with exponential slot edge for improved radiation pattern. *IEEE Antennas and Wireless Propagation Letters*, IEEE, v. 14, p. 1334–1337, 2015.

OLIVEIRA, A. M. de; JUSTO, J. F.; PEROTONI, M. B.; KOFUJI, S. T.; NETO, A. G.; BUENO, R. C.; BAUDRAND, H. A high directive k och fractal v ivaldi antenna design for medical near-field microwave imaging applications. *Microwave and optical technology letters*, Wiley Online Library, v. 59, n. 2, p. 337–346, 2017.

OLIVEIRA, A. M. de; JUSTO, J. F.; SERRES, A. J.; MANHANI, M. R.; MANIÇOBA, R. H.; PEROTONI, M. B.; BAUDRAND, H. Ultra-directive palm tree vivaldi antenna with 3d substrate lens for μ-biological near-field microwave reduction applications. *Microwave and Optical Technology Letters*, Wiley Online Library, v. 61, n. 3, p. 713–719, 2019.

SOBRINHO, R. E. F.; OLIVEIRA, A. M. de; NETO, A. M. De oliveira; SERRES, A. J. R.; ALEXANDRIA,

A. R. D.; PEROTONI, M. B.; NURHAYATI, N.; NOGUEIRA, I. C. et al. Vivaldi antipodal antenna with high gain and reduced side lobe level using slot edge with new neogothic fractal by cantor with application in medical images for tumor detection. *INAJEEE (Indonesian Journal of Electrical and Electronics Engineering)*, v. 3, n. 1, p. 25–31, 2020.

TENI, G.; ZHANG, N.; QIU, J.; ZHANG, P. Research on a novel miniaturized antipodal vivaldi antenna with improved radiation. *IEEE Antennas and Wireless Propagation Letters*, IEEE, v. 12, p. 417–420, 2013.

ZHU, S.; LIU, H.; CHEN, Z.; WEN, P. A compact gain-enhanced vivaldi antenna array with suppressed mutual coupling for 5G mmwave application. *IEEE Antennas and Wireless Propagation Letters*, IEEE, v. 17, n. 5, p. 776–779, 2018.